ROYAL SOCIETY OF CHEMISTRY

PAPER

Check for updates

Scavenging neurotoxic aldehydes using lysine carbon dots†

Daniel Nir Bloch,‡[a] Michele Sandre, ‡[bc] Shani Ben Zichri,[a] Anna Masato,[cd] Sofiya Kolusheva,[e] Luigi Bubacco*[cd] and Raz Jelinek *[ae]

Reactive aldehydes generated in cells and tissues are associated with adverse physiological effects. Dihydroxyphenylacetaldehyde (DOPAL), the biogenic aldehyde enzymatically produced from dopamine, is cytotoxic, generates reactive oxygen species, and triggers aggregation of proteins such as α-synuclein implicated in Parkinson's disease. Here, we demonstrate that carbon dots (C-dots) prepared from lysine as the carbonaceous precursor bind DOPAL molecules through interactions between the aldehyde units and amine residues on the C-dot surface. A set of biophysical and *in vitro* experiments attests to attenuation of the adverse biological activity of DOPAL. In particular, we show that the lysine-C-dots inhibit DOPAL-induced α-synuclein oligomerization and cytotoxicity. This work underlines the potential of lysine-C-dots as an effective therapeutic vehicle for aldehyde scavenging.

Introduction

Over the last few years, several studies reported on the involvement of catabolic aldehydes in the pathogenesis and progression of neurodegenerative disorders such as Parkinson's disease (PD), the most common movement disorder affecting two percent of the population worldwide over 65 years old.[1] PD is characterized by a multifactorial pathology, and accumulation of reactive aldehydes is perceived as a major etiopathogenic factor.[2] The dopamine metabolite 3,4-dihydroxyphenylacetaldehyde (DOPAL) has been identified as a prominent aldehyde species generated in PD by enzymatic degradation of dopamine.[3] Aldehydes usually react with amino groups of lysine residues, leading to covalent adducts, protein cross-linking and aggregation, thus compromising cellular homeostasis.[4]

The aggregation of the pre-synaptic protein α-synuclein (α-Syn) represents a distinctive trait of PD pathology.[5] Of note, α-Syn has been proposed as a preferential target for aldehydes being an intrinsically disordered protein, with a high percentage of lysine residues in its sequence.[6] Specifically in

dopaminergic neurons, the progressive DOPAL build-up resulting from a dysfunctional dopamine metabolism in PD[3] promotes the DOPAL covalent modification of α-Syn,[7,8] which has been demonstrated to alter synaptic vesicle organization and mobility.[7,8] Moreover, DOPAL triggers α-Syn off-pathway oligomerization, generating toxic species which contribute to dopaminergic synapse degeneration.[9] In this context, scavengers of catabolic reactive aldehydes have been studied, including small molecules such as metformin.[10,11]

Carbon dots (C-dots) are carbon-based nanoparticles exhibiting interesting physicochemical properties, including broad spectral fluorescence,[12] low cytotoxicity,[13,14] and biocompatibility.[15] An important feature of C-dots is the retaining of functional residues originating from the molecular building blocks on their surface due to the mild synthesis conditions, especially low reaction temperatures. This "structural memory" has been previously employed for modulating the surface properties of C-dots and targeting of the particles towards varied biological and chemical species.[14,16–18] C-dots have been used in a wide range of applications such as bioimaging,[16,19,20] chemical and biological sensing,[21–23] catalysis,[24,25] and others.[26]

Here, we demonstrate that C-dots prepared from lysine as the carbonaceous precursor interact with DOPAL, consequently inhibiting the adverse biological effects of the aldehyde. These effects are likely due to the abundant amine residues on the C-dot surface. In particular, the experimental data reveal that the lysine-C-dots can react with DOPAL intracellularly and inhibit its cytotoxicity. In addition, the lysine-C-dots can reduce the effect of DOPAL on α-Syn oligomerization, thus potentially minimizing the peptide-induced pathogenicity.

[a]Department of Chemistry, Ben Gurion University of the Negev, Israel. E-mail: razj@bgu.ac.il

[b]Department of Neuroscience, University of Padova, Italy

[c]Centro Studi per la Neurodegenerazione (CESNE), University of Padova, Italy. E-mail: luigi.bubacco@unipd.it

[d]Department of Biology, University of Padova, Italy

[e]Ilse Katz Institute for Nanoscale Science and Technology (IKI), Ben Gurion University of the Negev, Israel

† Electronic supplementary information (ESI) available. See DOI: https://doi.org/10.1039/d2na00804a

‡ Equally contributed to this work.

Experimental methods

Materials

L-Lysine (L-Lys) 99%, was purchased from Chem-Impex Int'l. Inc. Sucrose, thioflavin T (ThT), sodium carbonate and sodium bicarbonate were purchased from Sigma-Aldrich. N-TEMPO, 1,2-dimyristoyl-*sn*-glycero-3-phosphocholine (DMPC), 1-palmitoyl-2-oleoyl-*sn*-glycero-3-phosphoethanolamine (POPE), 2-dimyristoyl-*sn*-glycero-3-phospho-(1′-*rac*-glycerol) (DMPG), 1,2-dioleoyl-*sn*-glycero-3-phosphocholine (DOPC), 1,2-dioleoyl-*sn*-glycero-3-phosphoethanolamine (DOPE) and 1,2-dioleoyl-*sn*-glycero-3-phospho-L-serine (DOPS) were purchased from Avanti. Ethylene glycol was purchased from Alfa Aesar, hexafluoro-2-propanol (HFIP) was purchased from Apollo Scientific, and ethanol and diethyl ether were purchased from Bio Lab Ltd. 1-(4-Trimethylammoniumphenyl)-6-phenyl-1,3,5-hexatriene (TMA-DPH) was obtained from Interchim, Inc. and L-(−)-epinephrine, 99% was purchased from Acros organics and Sigma-Aldrich.

Carbon-dot synthesis

C-dots were prepared by a one-pot hydrothermal synthesis procedure. 1.0 g of L-Lys was dissolved in 10 mL of ethylene glycol and sonicated for 5 minutes in a sonication bath. The solution was then transferred to a poly(tetrafluoroethylene) (Teflon)-lined autoclave, and hydrothermal heating was carried out at 175 °C for 3.5 h. Thereafter, the C-dots were purified by dialysis in deionized water. Subsequently, the carbon dot solution was subjected to lyophilization, and the dried powder was re-dissolved in MQ water at a concentration of 10 mg mL^{-1}.

Recombinant α-synuclein expression and purification

Recombinant human α-Syn (1–140) was expressed and purified as previously described.[27] Briefly, the pET-28a-α-Syn plasmid was transformed into the *Escherichia coli* BL21(DE3) strain and α-Syn expression was induced with 0.1 mM isopropyl β-D-1-thiogalactopyranoside (IPTG). Cells were then collected by centrifugation and recombinant proteins were recovered from the periplasm by osmotic shock. After boiling the periplasmic homogenate, the α-Syn-containing fraction was subjected to two-step (35 and 55%) ammonium sulfate precipitation. The pellet was then resuspended and extensively dialyzed against water. Subsequently, the protein was purified by fast protein liquid chromatography using a Resource Q column (Amersham Biosciences) and eluted with a 0–1 M gradient of NaCl in 30 minutes. Proteins were then dialyzed against water, lyophilized, and stored at −20 °C. Once resuspended in PBS for experiments, the α-Syn solution was filtered through an Amicon Ultra centrifugal filter unit (MWCO 100 kDa) to eliminate oligomeric species induced by the lyophilization step. Protein concentration was finally determined by measuring absorbance at 276 nm ($\varepsilon = 5.8$ cm^{-1} mM^{-1}).

DOPAL synthesis

DOPAL was synthesized from (±)-epinephrine hydrochloride according to Fellman's protocol.[28] After extraction from ethyl acetate, DOPAL was resuspended in MQ water. DOPAL concentration was determined by assuming the same extinction molar coefficient of DA and L-DOPA ($\varepsilon_{280} = 2.63$ cm^{-1} mM^{-1}) and the quality of the preparation was analyzed by reverse-phase HPLC on a Phenomenex Jupiter column (300 Å/5 μm, 250 mm × 4.6 mm), using linear gradients of solvent B in eluent A (A: 0.1% TFA in H$_2$O, B: 0.08% TFA in acetonitrile; gradient: 5% B to 65% B in 20 minutes).

In vitro DOPAL-induced α-synuclein oligomerization and inhibition by lysine-C-dots

Oligomers were produced by incubating recombinant α-Syn to a final concentration of 20 μM with 300 μM DOPAL in PBS, in a 1 : 15 α-Syn : DOPAL ratio, which corresponds to 1 : 1 lysine : aldehyde. C-dots were added to the solution at the indicated amount (μg). The solutions were then incubated for 2 hours by shaking at 350 rpm at 37 °C. At the endpoint of incubation, 30 μL of each sample (10 μg of α-Syn) were collected and the reactions were stopped by the addition of loading buffer. Monomeric α-Syn and α-Syn oligomers were then resolved by SDS-PAGE into a gradient 4–20% SDS-PAGE gel (GenScript). The gel was scanned on a LiCor Odissey for the near infrared fluorescence signal at 800 nm, and then stained with Coomassie brilliant blue (0.15% Coomassie Brilliant Blue R and 40% ethanol), followed by destaining with 10% isopropanol and 10% acetic acid. Image analysis was then performed with Fiji software.

SH-SY5Y stable cell line generation, maintenance, and manipulation

Neuroblastoma-derived SH-SY5Y cells (ATCC CRL-2266) were cultured in 50% Dulbecco's modified Eagle's medium (DMEM, Biowest) and 50% F-12 Nutrient Mix (Biowest) supplemented with 10% v/v FBS (Corning) and 1% Penicillin/Streptomycin (Biowest). Alternatively, SH-SY5Y neuroblastoma cell lines were a generous gift from Prof. Niv Papo (BGU) and were grown at 37 °C and in 5% CO$_2$ in DMEM supplemented with 10% tetracycline-free fetal bovine serum (FBS), L-glutamine (2 mM), and penicillin (100 units per mL)/streptomycin (0.1 mg mL^{-1}) (Biological Industries, Israel).

To generate an α-Syn-EGFP overexpressing stable cell line, SH-SY5Y cells were transduced with lentiviral particles encoding α-Syn-EGFP generated at the BSL2 DiBio facility (UNIPD). Briefly, α-Syn-EGFP gene7 was cloned in a pLKO DEST hygro lentiviral vector (Addgene). HEK293FT cells were co-transfected with pLKO α-Syn-EGFP hygro, pdR8.2 (Addgene) and pVSV-G plasmids (Addgene) for three days. Lentiviral particles were then collected from the cell medium by ultracentrifugation at 50 000g for 2 hours at 4 °C. The pellet was then resuspended in PBS supplemented with 5% BSA. SH-SY5Y cells at 40% confluency were transduced with pLKO α-Syn-EGFP hygro lentiviral particles for 72 hours, following positive selection with 200 μg mL^{-1} hygromycin (Roth). Cell treatment with different concentrations of DOPAL and C-dots were performed in Opti-MEM (Life Technologies) for the indicated amount of time.

Morphological cell analysis by giemsa staining

SH-SY5Y cells were seeded in 12-well plates (Sarstedt) at a density of 8.0×10^4 cells per well and maintained in an incubator for 24 hours. Cells were pre-treated with Lys C-dots for 24 hours, following DOPAL treatment for 18 hours without medium change. Cells were then rinsed twice with PBS and fixed with 100% methanol for 2 minutes following 4% paraformaldehyde in PBS for 15 min. After washing with PBS, a Giemsa (Sigma) stock solution was diluted 1 : 10 in PBS and added to the fixed cells for 20 minutes in the dark.[29] Finally, cells were washed with water, dried, and imaged on a Leica DMI4000 B inverted microscope in bright field. In each field of view, the number of dark rounded cells per unit area (μm^2) was quantified.

SDS-PAGE and western blot

After treatment, α-Syn-EGFP expressing SH-SY5Y cells were harvested in RIPA buffer (Cell Signaling Technology) supplemented with protease inhibitor cocktail (Roche). Lysates were clarified by centrifugation at 20 000g at 4 °C. Protein concentration in the clear supernatant was determined using the Pierce® BCA protein assay kit (Thermo Scientific) following the manufacturer's instructions and protein samples were loaded on gradient 4–20% tris-MOPS-SDS gels (GenScript). Proteins were then transferred to PVDF membranes (Bio-Rad), through a semi-dry Trans-Blot® Turbo™ transfer system (Bio-Rad). PVDF membranes were subsequently blocked in tris-buffered saline plus 0.1% Tween (TBS-T) and 5% no-fat dry milk for 1 hour at room temperature and then incubated overnight at 4 °C with primary antibodies. The following primary antibodies were used: anti-HSP90 (05-594, Sigma-Aldrich), anti-HSP70 (SAB4200714, Sigma-Aldrich), anti-αSyn MJFR1 (ab138501, Abcam), and anti-β-Actin (A1978, Sigma-Aldrich). After incubation with HRP-conjugated secondary antibodies (Sigma-Aldrich) at room temperature for 1 hour, immunoreactive proteins were visualized using an Immobilon® Forte Western HRP substrate (Millipore) on an Imager CHEMI Premium detector (VWR). The densiometric analysis of the detected bands was performed by using the Fiji software.

Confocal imaging and immunofluorescence

After treatment, α-Syn-EGFP expressing SH-SY5Y cells were fixed with 4% paraformaldehyde for 20 minutes at room temperature. After permeabilization with 0.3% Triton-X (Sigma-Aldrich) in PBS for 5 minutes and saturation with 5% FBS in PBS for 1 hour at room temperature, fixed cells were incubated with an anti-α-Syn MJFR1 (ab138501, Abcam) primary antibody overnight at 4 °C. After incubation with an Alexa Fluor-568-conjugated anti-rabbit secondary antibody (Invitrogen) for 1 hour at room temperature, nuclei were stained with Hoechst 33 258 (Invitrogen) 1 : 2000 in PBS for 10 minutes, following mounting of coverslips on glass slides with Mowiol. Cell imaging was performed on a Leica 5000B epifluorescence microscope.

For the internalization study of C-dots, cells were seeded on 0.8 cm² micro-slides (Nunc™ Lab-Tek™, ThermoFisher Scientific, USA) at a density of 2×10^4 cells per well and maintained overnight. For monitoring the penetration of the Lys C-dots into the cells, the SH-SY5Y cells were incubated with 2.5 mg mL^{-1} C-dots. Following 20 h of incubation of the cells with the C-dots, images of live cells were acquired on a Zeiss LSM880 confocal microscope (Germany), using a CLSM plan-Apochromat, ×20/0.8 M27 objective or ×60/1.35 numerical aperture oiled-immersion objective. Excitation/emission wavelengths were 405/561 nm.

Protein and sample preparations

α-Syn was dissolved in HFIP containing a few drops of concentrated ammonium hydroxide at a concentration of 1 mg mL^{-1} and stored at −20 °C until use to prevent aggregation. For each experiment (ThT, TEM, CD and fluorescence anisotropy) the solution was thawed, and the required amount was dried by evaporation for 5–6 h to remove HFIP. The dried peptide sample was dissolved in 10 mM sodium phosphate buffer (PB) pH 7.4 at room temperature.

Isothermal titration calorimetry (ITC)

The lysine-C-dots were diluted to a final concentration of 1.0 mg mL^{-1} and the titration syringe was filled with the sample of the C-dots. A sample of 1.5 mL of the DOPAL 1 mM solution or 1.5 mL of the buffer was inserted into the Nano ITC cell (TA Instruments, Newcastle, DE) and the cell was heated to 37 °C. After equilibrium was reached, injection of 5 μL aliquots was carried out every 350 s.

DOPAL effects on C-dot fluorescence

The C-dot solution (0.5 mg mL^{-1}) was titrated with DOPAL (concentrations from 0.0007 mg mL^{-1} to 1.55 mg mL^{-1}) and each sample was incubated for 1 hour. A 150 μL aliquot of the mixture was placed in a 96-well plate and C-dot fluorescence was measured in the wavelength demonstrating the maximum emission of the C-dots alone. The excitation was carried out at 350 nm, and emission was measured at 430 nm which is the wavelength exhibiting the maximum emission for the C-dots according to the excitation emission dependence of the C-dots.

Preparation of small unilamellar vesicles (SUVs)

Lipid components [DOPC, POPE/DMPG (50 : 50), or DOPC/DOPE/DOPS (60 : 25 : 15)] were dissolved in a mixture of chloroform/ethanol (1 : 1) and dried under vacuum to constant weight, followed by addition of phosphate buffer (pH 7.4). For each experiment, vesicles were freshly prepared by probe-sonication of the phospholipid suspension for 10 min at room temperature, with 20% amplitude and on/off 59 s cycles according to a previously published protocol. For all experiments, the final total concentration of lipids was 1 mM, except for the ESR experiment, in which the final lipid concentration was 10 mM.

ThT fluorescence kinetic assay

ThT fluorescence measurements were carried out at 37 °C using a 96-well black plate on a Biotek Synergy H1 plate reader. Measurements were made on a sample containing 70 μM α-Syn

in the absence or presence of DOPAL (350 mM) and lysine-C-dots at a concentration of 0.5 mg mL^{-1}. 150 µL aliquots of the aggregation reaction were mixed with 10 µM ThT in 10 mM phosphate buffer (pH 7.4). A single glass bead was placed in each well and the plate was shaken continuously. The fluorescence emission was measured every 5 min for 34 h at $\lambda_{ex} = 440$ and $\lambda_{em} = 485$ nm. The self-fluorescence of the C-dots was subtracted from the measured fluorescence for each sample. Results are presented as means ± SD for each sample.

Transmission electron microscopy (TEM)

5 µL aliquots from samples used in the ThT experiments (after 34 h incubation) were placed on 400-mesh copper grids covered with a carbon-stabilized Formvar film. Excess solutions were removed following 2 min of incubation, and the grids were negatively stained for 30 s with a 1% uranyl acetate solution. Samples were viewed in an FEI Tecnai 12 TWIN TEM operating at 120 kV.

Circular dichroism (CD) spectroscopy

CD spectra were recorded in the range of 200–260 nm at room temperature on a Jasco J-715 spectropolarimeter, using 1 mm quartz cuvettes. The samples containing α-Syn in the absence or presence of DOPAL and Lys C-dot where preincubated for 24 hours and then introduced into DOPC/DOPE/DOPS (60 : 25 : 15) SUVs. 'Final 400 µL solutions contained 70 µM α-Syn, 350 µM DOPAL and 0.5 mg mL^{-1} Lys C-dots. Spectra were recorded immediately after the addition of the SUVs and after 24 h of incubation with the SUVs. The CD signals resulting from SUVs, DOPAL and C-dots were subtracted from the corresponding spectra.

Fluorescence anisotropy

The fluorescence probe TMA-DPH was incorporated into the POPE/DMPG SUVs (50 : 50) by adding the dye dissolved in THF (1 mM) up to a final concentration of 1.25 µM. After 30 min of incubation of TMA-DPH at 25 °C, fluorescence anisotropy was measured at $\lambda_{ex} = 360$ nm and $\lambda_{em} = 430$ nm using an FL920 spectrofluorometer (Edinburgh Co., Edinburgh, UK). Data were collected before and after the addition of freshly prepared mixtures of α-Syn with DOPAL and Lys C-dot and after incubation of 24 hours; as control measurements we measured the effect of α-Syn alone and the effect of DOPAL alone. Anisotropy values were automatically calculated using a spectrofluorometer. The software uses the equation: $r = (I_{VV} - GI_{VH})/(I_{VV} + 2GI_{VH})$, $G = I_{HV}/I_{HH}$, in which I_{VV} corresponds to excitation and emission polarizers mounted vertically; I_{HH} corresponds to excitation and emission polarizers mounted horizontally; I_{HV} is the excitation polarizer mounted horizontally and the emission polarizer mounted vertically; I_{VH} requires the excitation polarizer mounted vertically and emission polarizer mounted horizontally. Results are presented as means ± standard error of the mean (SEM) of seven replicates.

Atomic force microscopy (AFM)

The C-dot aqueous solution (80 µL, 0.05 mg mL^{-1}) was deposited on a silicon wafer and scanned by AFM under wet conditions (Cypher ES, Asylum Research, Oxford Instruments, Goleta, CA) in tapping mode. All images were acquired using a silicon probe (AC 40, Olympus) under the following conditions: spring constant of 2 N m^{-1}, a frequency of 25 kHz, and a tip radius of 9 nm.

FTIR microscope

5 µL aliquots of the samples containing lysine-C-dots or the Lys precursor used in the C-dot synthesis were transferred to an aluminium coated slide and dried under vacuum. FTIR spectra were recorded using an iN10 FTIR microscope (Thermo Fisher Scientific, USA) fitted with a liquid N2–S4 cooled mercury cadmium telluride A (MCTA) detector. Spectra were recorded in the range 4000–700 cm^{-1} at 8 cm^{-1} resolution, with 64 scans averaging and a minimal measuring area of 30 × 30 µm^2.

Fluorescence spectroscopy

Fluorescence emission spectra of the C-dot solution were recorded on an FL920 spectro-fluorometer (Edinburgh Instruments, Livingston, UK). Fluorescence emission spectra were acquired in the range of 300–800 nm with different excitations. The fluorescence was measured at a 90° angle relative to the excitation light. This geometry is used instead of placing the sensor at the line of the excitation light at a 180° angle to avoid interference of the transmitted excitation light.

Results and discussion

This study aims at assessing the effect of lysine-C-dots on the reactivity and cytotoxicity of DOPAL, a potent cytotoxic aldehyde. Fig. 1 depicts characterization of the lysine C-dots, synthesized by a simple hydrothermal process using lysine as the carbonaceous building block. Fig. 1A shows the excitation-dependent emission spectra of the Lys-C-dots, highlighting the maximal emission at approximately 420 nm upon excitation at 350 nm. Excitation-dependence of the fluorescence emission is a distinctive property of C-dots.

The representative atomic force microscopy (AFM) image of surface-deposited C-dots in Fig. 1B highlights the relative homogeneity of the carbon nanoparticles, exhibiting on average a diameter of 5 ± 1 nm. The Fourier transform infrared (FTIR) spectra of the Lys-C-dots in Fig. 1C (black spectrum), in comparison to those of pure lysine (Fig. 1C, red) indicate that lysine functional units were retained on the C-dot surface. Specifically, the peak at around 1100 cm^{-1} is ascribed to C–N stretching of Lys residue while N–H bands corresponding to lysine side chains are at around 3340 cm^{-1}, 2930 cm^{-1}, and 1550 cm^{-1}.

A key question addressed in this work is whether specific interactions occur between the synthesized lysine-C-dots and DOPAL, and whether such interactions have an impact on the biological effects of DOPAL. Fig. 2 presents spectroscopic and thermodynamic experiments designed to evaluate the interactions between the Lys-C-dots and DOPAL. Fig. 2A depicts the fluorescence intensity (excitation at 350 nm; emission at 430 nm) of Lys-C-dots recorded upon addition of increasing
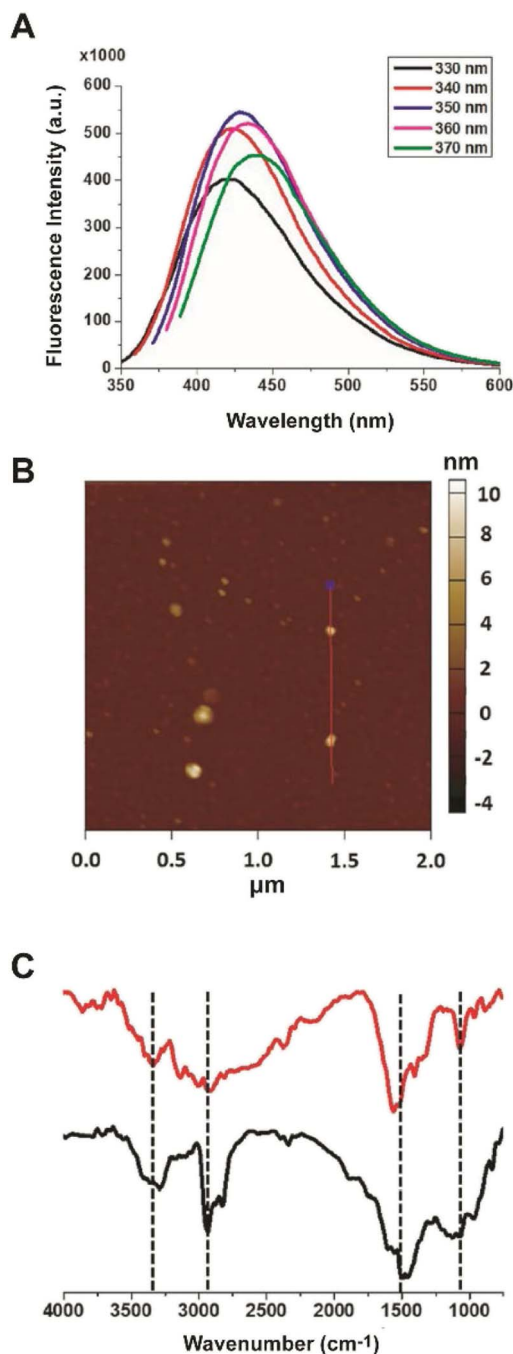
Fig. 1 C-dot characterization. (A) PL emission spectra of the Lys C-dots upon excitation at different wavelengths (330–370 nm). (B) Representative AFM image showing Lys C-dots. The FTIR spectra (C) of the Lys C-dots. The peaks at ~3340 cm^{-1}, 2935 cm^{-1}, and 1560 cm^{-1} are ascribed to N–H stretching, and the peak at ~1068 cm^{-1} is ascribed to C–N stretching.
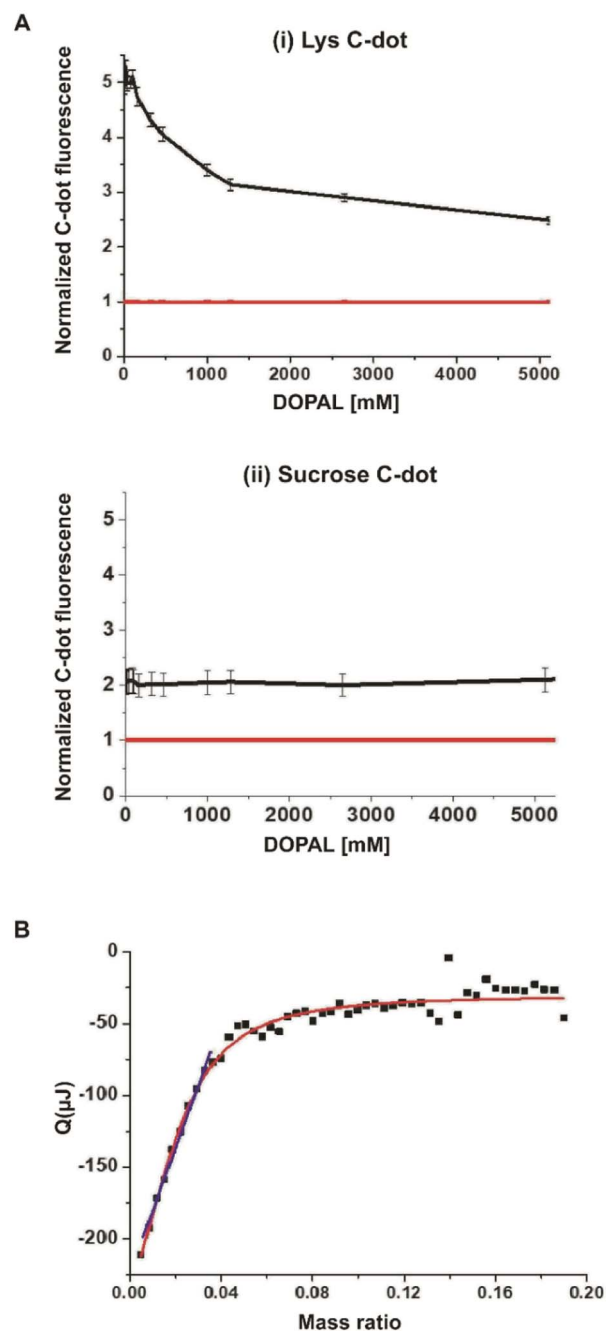
Fig. 2 Interaction between Lys C-dots and DOPAL. Quenching effects upon exposure to increasing concentrations of DOPAL for Lys C-dots (A, i) and sucrose C-dots (A, ii), both shown in the black line at the corresponding images, normalized to the fluorescence of DOPAL as demonstrated by the quenching effect of increasing concentrations of DOPAL. The red line shows the fluorescence of DOPAL. C-dot concentration is 0.5 mg mL^{-1}. (B) The model fit of interaction between the Lys C-dots and DOPAL as measured by ITC. Lys C-dots (1 g mL^{-1}) and DOPAL (10 mM).

concentrations of DOPAL. Indeed, the fluorescence emission was quenched as the DOPAL concentration was increased, accounting for C-dot/DOPAL binding. Numerous studies have shown significant attenuation of C-dot fluorescence following binding to other molecular entities.[30,31] In contrast, the fluorescence emission of C-dots, that were prepared from sucrose as

the carbonaceous building block, was not altered upon addition of DOPAL (Fig. 2A(ii)), confirming the selective targeting of Lys-C-dots by DOPAL. Sucrose was selected as the control C-dot precursor as it does not contain amine groups which may

react with DOPAL. The isothermal titration calorimetry (ITC) analysis in Fig. 2B further confirms the occurrence of significant interactions between the Lys-C-dots and DOPAL. The ITC curve indicates exothermal interaction between DOPAL and the Lys-C-dots. The interaction curve reveals an approximate 20 : 1 weight ratio between bound DOPAL molecules and the Lys-C-dots, and the linear component of the curve yields a binding constant of 4750 ± 100.

As the Lys-C-dots exhibit significant interactions with DOPAL (*e.g.*, Fig. 2), we next assessed whether the C-dots inhibit DOPAL-induced cell toxicity (Fig. 3). We first evaluate the behaviour of Lys C-dots with cell cultures. As showed in Fig. SI-1A,† the addition of Lys C-dots to the cell culture medium results in Lys C-dot permeation within the neuroblastoma-derived SH-SY5Y cells. After 20 hours of incubation, Lys C-dots can be detected by confocal microscopy taking advantage of Lys C-dot intrinsic fluorescence, whose signal overlaps with the bright field image of the cells. Moreover, the administration of Lys C-dots at different concentrations up to 2.5 mg mL^{-1} for 24 hours did not affect the SH-SY5Y cell viability (Fig. SI-1B),† coherently with previous reports.[18]

In the experiments, the cells were treated for 24 h with 100 μM DOPAL in combination with increasing concentrations of Lys-C-dots (0.2–0.4–0.8–1.6 mg mL^{-1}). The effect on cell viability was then measured. As a control measurement, the effect of DOPAL and the C-dots at the highest concentration was tested as well. The cell viability diagram in Fig. 3, obtained through application of the XTT assay using SH-SY5Y cells, reveals that incubation with DOPAL (100 μM) induces ∼30% death in the cell population. Conversely, co-incubation of the DOPAL/cell mixtures with Lys-C-dots blocked DOPAL-induced toxicity, demonstrating a C-dot concentration-dependent increase in cell viability. Indeed, Fig. 3 shows that 1.6 mg mL^{-1} Lys C-dots effectively restored a cell viability value comparable to that of control cells (untreated with DOPAL).

A similar cell viability outcome is apparent in the microscopy analysis of SH-SY5Y cells by Giemsa staining, reporting their chromatin condensation st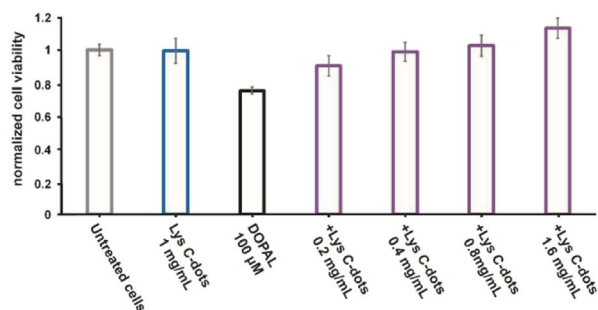atus by an increased Giemsa violet colour stain. Indeed, the morphological analysis in Fig. 4A confirms significant chromatin condensation accounting for apoptotic cells[32] (darker and rounded cells, inset) after 18 hours of 150 μM DOPAL treatment, in combination with Lys-C-dots over a range of concentrations previously reported in astrocytes.[33] Notably, pre-treatment of the cells with the Lys-C-dots for 24 hours prior to DOPAL addition, well blocked DOPAL-induced cell death, notably reducing the number of rounded (apoptotic) cells (Fig. 4A). The cell morphology analysis in Fig. 4B further confirms that the Lys-C-dots alone did not adversely affect cell viability. Overall, the experiments presented in Fig. 3 and 4 attest to significant cell protective effects of Lys-C-dots in the case of DOPAL-induced cell death, and, furthermore, that the Lys-C-dots by themselves did not exhibit cell toxicity.

Interactions of α-Syn oligomers and fibrils with membranes have been linked to their pathological effects and cytotoxicity.[34–39] Fig. 5 examines the effects of the Lys-C-dots upon DOPAL-induced modulation of the α-Syn secondary structure and lipid bilayer interactions. Fig. 5A presents the circular dichroism (CD) spectra of α-Syn in lipid vesicle solutions (DOPC/DOPE/DOPS, at the 12 : 5:3 ratio).[7] Particularly interesting is the effect of DOPAL or a Lys C-dot/DOPAL mixture on the vesicle-affected peptide conformation. The CD spectrum of α-Syn in the DOPE/DOPC/DOPS vesicle solution reveals the features of a typical helical conformation exhibiting a saddle-like shape with minima at ∼225 nm and ∼210 nm (ref. 40) (Fig. 5A, black spectrum). When DOPAL is added to the α-Syn/vesicle solution, however, the peptide conformation became largely random exhibiting a single minimum at 200 nm (Fig. 5A, grey spectrum). This observation indicates that DOPAL hinders the helical-inducing interactions between the vesicle bilayers and α-Syn. Notably, when the Lys-C-dots were also included in the DOPAL/α-Syn/lipid vesicle solution, the helical conformation of the protein was retained (Fig. 5A, blue spectrum), likely as a consequence of the scavenging effect of the C-dots on the aldehyde, complementing the previous experimental data.

The fluorescence anisotropy data in Fig. 5B report on the effect of DOPAL or the DOPAL/Lys-C-dot mixture upon lipid bilayer interactions of α-Syn. In the experiment, we used vesicles comprising POPE and DMPG and the fluorescent marker trimethylamine-diphenylhexatriene (TMA-DPH) at a 1 : 1 : 0.002 molar ratio (POPE : DMPG : TMA-DPH). The fluorescence anisotropy of TMA-DPH has been widely used as a tool to measure bilayer fluidity in vesicular systems and its modification following interactions of membrane-active species.[41,42] When α-Syn alone was added to the lipid vesicles, the fluorescence anisotropy decreased with time (Fig. 5B, left bars) from 0.255 initially to 0.247 after 24 hours, reflecting the increase in membrane fluidity upon addiction of the protein. When DOPAL was co-added with α-Syn to the vesicles, significantly higher fluorescence anisotropy was recorded (Fig. 5B, middle bars), accounting for increased rigidity of the membrane. Yet, echoing the trend observed for α-Syn alone, a decrease in membrane fluidity occurred after 24 h, ascribed to aggregation of α-Syn in the presence of the aldehyde. Notably, when both DOPAL and Lys-C-dots were co-incubated with α-Syn, the anisotropy was

Fig. 3 Toxicity of DOPAL and the protective effect of Lys C-dots in the neuronal SH-SY5Y cells were studied by XTT assay. The left side shows the viability of the cells in the medium (grey histogram), in the presence of 100 μM DOPAL (black histogram), and in the presence of 1 mg mL^{-1} Lys C-dots (blue histogram); the right section shows the effect of increasing concentrations of Lys-C-dots on cell viability in the presence of 100 μM DOPAL (purple histograms).
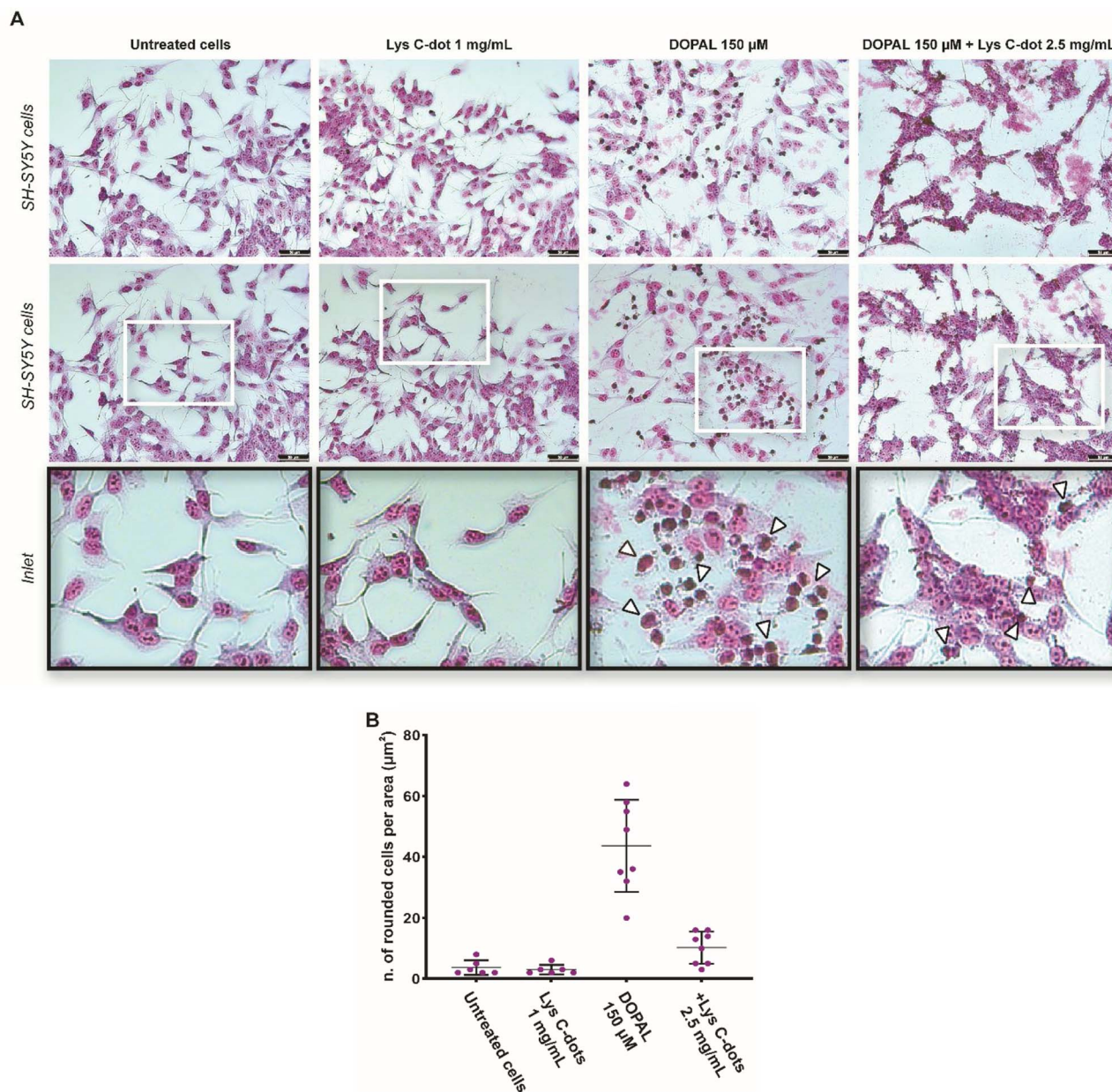
Fig. 4 Protective effect of Lys C-dots against DOPAL-induced cytotoxicity in SH–SY5Y cells. (A) Cell morphology analysis by Giemsa staining. Representative bright field images and relative high magnification images (inset) are shown. DOPAL toxicity results in accumulation of rounded cells (black outlined white arrowheads) per unit area, whereas pre-treatment with 2.5 mg mL^{-1} Lys C-dots reduced the DOPAL effect. (B) Quantification of the number of rounded cells per unit area (μm^2) was performed in $n = 10$ images for each condition and data are showed as mean $\pm$ SEM. Scale bar: 50 μm.

considerably reduced due to interactions of the C-dots with the vesicles, however, no change in the anisotropy of DMA-DPH was apparent after 24 hours (Fig. 5B, right bars). This result likely indicates that α-Syn remains in the monomeric state and did not undergo aggregation.

In addition to the adverse effects on cell viability, DOPAL has been reported to trigger the formation of toxic α-Syn oligomers through covalent modification of the lysine residues within the peptide and protein cross-linking.[6–8] Accordingly, we examined the effects of the Lys-C-dots upon DOPAL/α-Syn interactions, α-Syn aggregation, and biological effects (Fig. 4–7). In the

experiments depicted in Fig. 6, we assessed the effects of the Lys-C-dots upon DOPAL-modulated aggregation of α-Syn. Fig. 6A depicts thioflavin-T (ThT) fluorescence emission curves accounting for α-Syn fibrillation kinetics. α-Syn alone gave rise to gradually increasing ThT fluorescence corresponding to fibril formation (Fig. 6A, black curve).[43–46] Co-addition of DOPAL to the α-Syn solution, however, significantly attenuated the ThT fluorescence (Fig. 6A, grey curve), attesting to inhibition of fibril formation and occurrence of off-pathway oligomerization instead.[3,6,8,47,48] Notably, when Lys-C-dots and DOPAL were added together to the α-Syn solution, ThT fluorescence
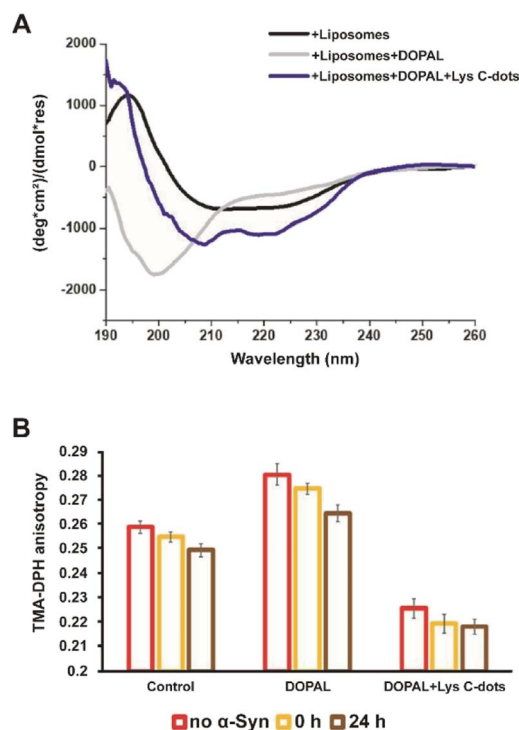
Fig. 5 Interactions between α-Syn and lipid liposomes in the presence of DOPAL and DOPAL + Lys C-dots. (A) The C-dots change the secondary structure of α-Syn in liposomes (60% DOPC, 25% DOPE, and 15% DOPS) as tested by CD spectra of α-Syn (10 μM) (black line), in the presence of DOPAL (300 μM) and liposomes (grey line), in the presence of DOPAL + Lys C-dots and liposomes (blue line). (B) The change in the anisotropy fluorescence of POPE/DMPG vesicles with time as tested by the TMA-DPH fluorescence marker in the presence and absence of 70 μM α-Syn in the presence of DOPAL and a combination of DOPAL + Lys C-dot. Each column represents the condition reported in the legend.

emission was partly restored (Fig. 6A, blue curve), likely indicating that the Lys-C-dots sequestrated DOPAL, thus promoting α-Syn self-assembly and fibrillation.

The transmission electron microscopy (TEM) images in Fig. 6B complement the ThT fluorescence data and shed further light on the effects of DOPAL and the Lys-C-dot/DOPAL mixture, respectively, upon α-Syn aggregation. α-Syn alone forms fibers very efficiently (Fig. 6B(i)), while the addition of DOPAL significantly inhibited fibril formation (Fig. 6B(ii)), echoing the ThT fluorescence data in Fig. 6A. In contrast, the TEM image in Fig. 6B(iii) reveals formation of α-Syn fibrils, corroborating the ThT analysis in Fig. 6A and attesting the Lys-C-dot capacity to block the fibrillation inhibitory effect of DOPAL.

To further characterize the impact of the Lys-C-dots on DOPAL-induced α-Syn oligomerization, we incubated recombinant α-Syn (20 μM) with DOPAL (300 μM) in a 1 : 15 molar ratio (protein : DOPAL; this ratio corresponds to the 1 : 1 molar ratio between the number of lysine and DOPAL molecules) with/without co-addition of Lys-C-dots (Fig. 7). The SDS-PAGE staining image (Fig. 7A) and corresponding quantitative band analysis (Fig. 7B) indicate that, after incubation for 2 hours at 37 °C in PBS pH 7.4, DOPAL induced formation of covalent α-
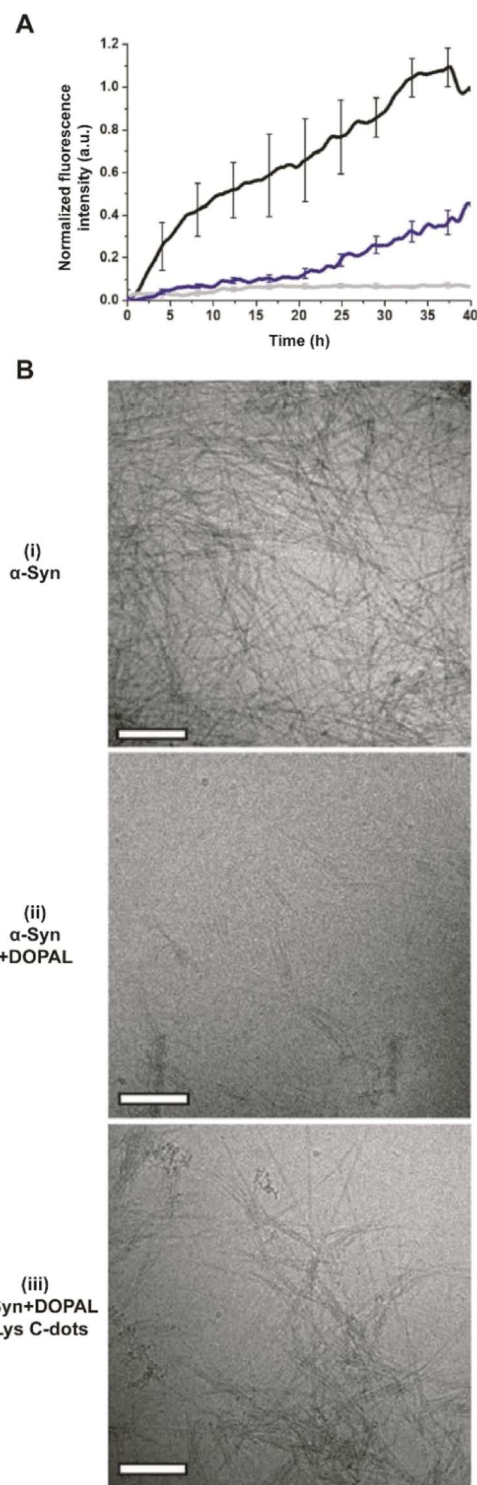

Fig. 6 DOPAL scavenging by Lys C-dots restores α-Syn fibrillation. (A) Graph shows the effect of 350 μM DOPAL (grey line) and Lys C-dots (0.7 mg mL^{-1}) + DOPAL (blue line) on α-Syn aggregation; black line - control (15 μM THT, 70 μM α-Syn, and 10 mM PB buffer). (B) TEM images of (i) α-Syn, (ii) α-Syn + DOPAL and (iii) α-Syn + DOPAL + Lys C-dots. Scale bar 200 nm.

Syn dimers and trimers.[8] Importantly, co-incubation of α-Syn and DOPAL with increasing concentrations of Lys-C-dots significantly inhibited α-Syn oligomerization by DOPAL in
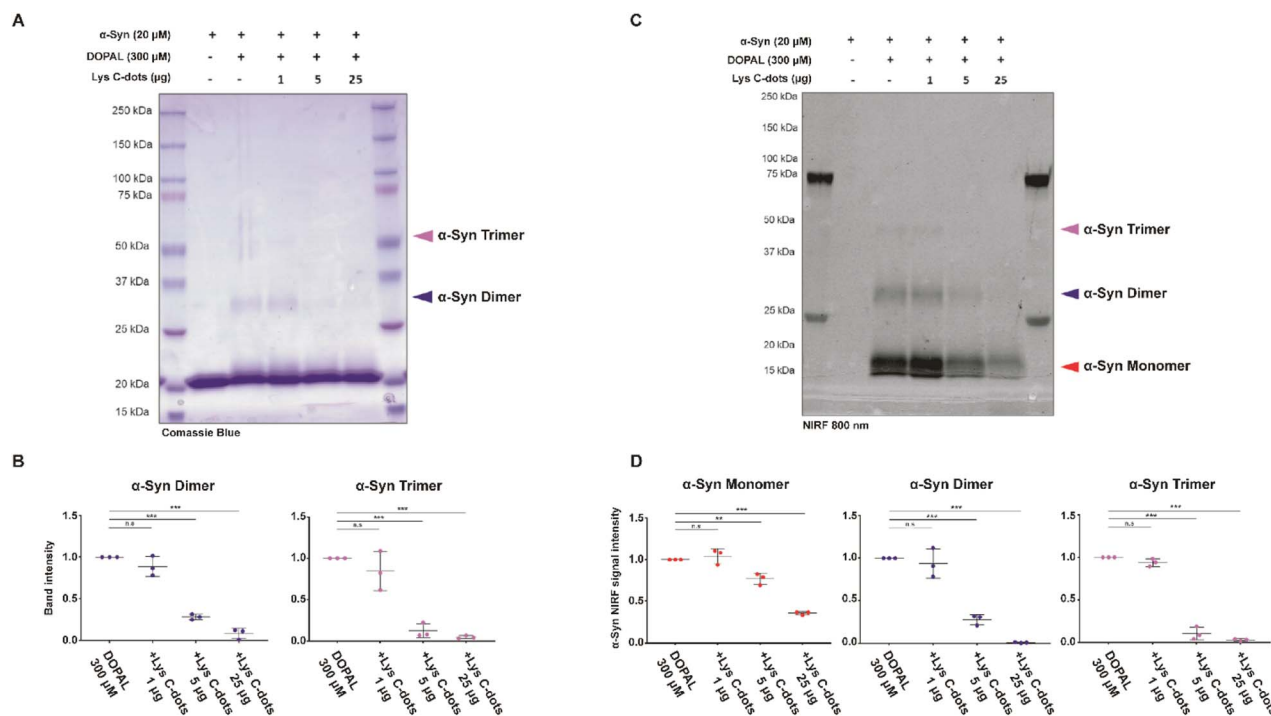
Fig. 7 Lys C-dots prevent DOPAL covalent modification of α-Syn lysines and protein aggregation. (A–C) *In vitro* aggregation assay of 20 μM α-Syn and 300 μM DOPAL at 350 rpm at 37 °C for 2 hours, in the presence of 0–1–5–25 μg of Lys C-dots. Oligomers were resolved in SDS-PAGE and an in-gel nIRF signal at 800 nm was detected prior to Coomassie staining. (B) Relative quantification of band intensity of α-Syn dimers and trimers in the Coomassie staining, as well as the (D) nIRF signal of α-Syn monomers, dimers, and trimers. Data are collected from three independent experiments, normalized to the relative band intensity in the α-Syn-DOPAL sample and presented as mean ± SEM. Statistical analysis was performed by the one-sample *t*-test (**$p < 0.01$, ***$p < 0.001$).

a dose-dependent fashion, as showed by the quantification of the band intensity at 30 kDa (***$p < 0.001$) and 45 kDa (***$p < 0.001$), which correspond to α-Syn dimers and trimers, respectively (Fig. 7B).

To prove that Lys-C-dots prevent DOPAL covalent modification of α-Syn lysines by scavenging the aldehyde, we took advantage of the near infrared fluorescence (nIRF) signal derived from oxidized catechol bound to proteins.[49] *In vitro* DOPAL modification on α-Syn lysines can occur by both the Schiff-base reaction with the aldehyde moiety and by the Michael addition on the oxidized catechol.[7] DOPAL-modified α-Syn monomers can form inter-molecular binding generating small dimeric, trimeric and tetrameric oligomers within 2 hours of incubation. Hence, we assessed the amount of DOPAL adduct formation and protein aggregation by in-gel detection of quinone-modified proteins based on nIRF at 800 nm (Fig. 7C). The nIRF analysis allows us to detect the quinone modification also on the monomeric form of the protein. The analysis reveals the presence of oxidized catechol adducts on α-Syn monomers (16 kDa), dimers (30 kDa) and trimers (45 kDa). However, when incubated with Lys-C-dots, the nIRF signal derived from DOPAL adducts on the α-Syn monomer and oligomeric species presents a significant dose-dependent decrease (Fig. 7D).

Specifically, DOPAL modification on the α-Syn monomer decreases to ∼23% and ∼64% in the presence of 5 μg and 25 μg of Lys C-dots respectively, while the nIRF signal on both α-Syn

dimers and trimers almost completely disappeared (∼99% and ∼97%) in the presence of 25 μg, and with less yield (∼72% and ∼89%) with 5 μg of Lys C-dots (Fig. 7D).

We additionally investigated the capability of Lys-C-dots to scavenge DOPAL and prevent DOPAL-induced α-Syn oligomerization in SH-SY5Y cells (Fig. 8). In the experiments, we employed SH-SY5Y cells over-expressing α-Syn-EGFP as the α-Syn-EGFP dimeric form can be easily detected by western blot.[8] Fig. 8A depicts immunofluorescence microscopy images underscoring co-localization of the EGFP fluorescence signal with the anti-α-Syn immunostaining, thereby confirming intracellular expression of α-Syn-EGFP. Next, we sought to assess the effect of DOPAL on α-Syn-EGFP oligomer formation. The western blot analysis of α-Syn-EGFP OE SH-SY5Y cells incubated with progressively increasing DOPAL concentrations (100–200 μM) for 16 and 24 hours reveals a band between 90 and 100 kDa corresponding to the α-Syn-EGFP dimer (Fig. 8B). The band at the apparent molecular weight of ∼45 kDa indicates the α-Syn-EGFP monomer protein, which is characterized by a high degradation rate denoted by a smeared signal at lower molecular weights.

Based on this experimental setup, we assessed the impact of the Lys-C-dots upon intracellular DOPAL-induced α-Syn oligomerization (Fig. 8C). SH-SY5Y cells over-expressing α-Syn-EGFP were pre-treated for 24 hours with Lys-C-dots prior to addition of DOPAL (150 μM). Indeed, the WB data (quantitative
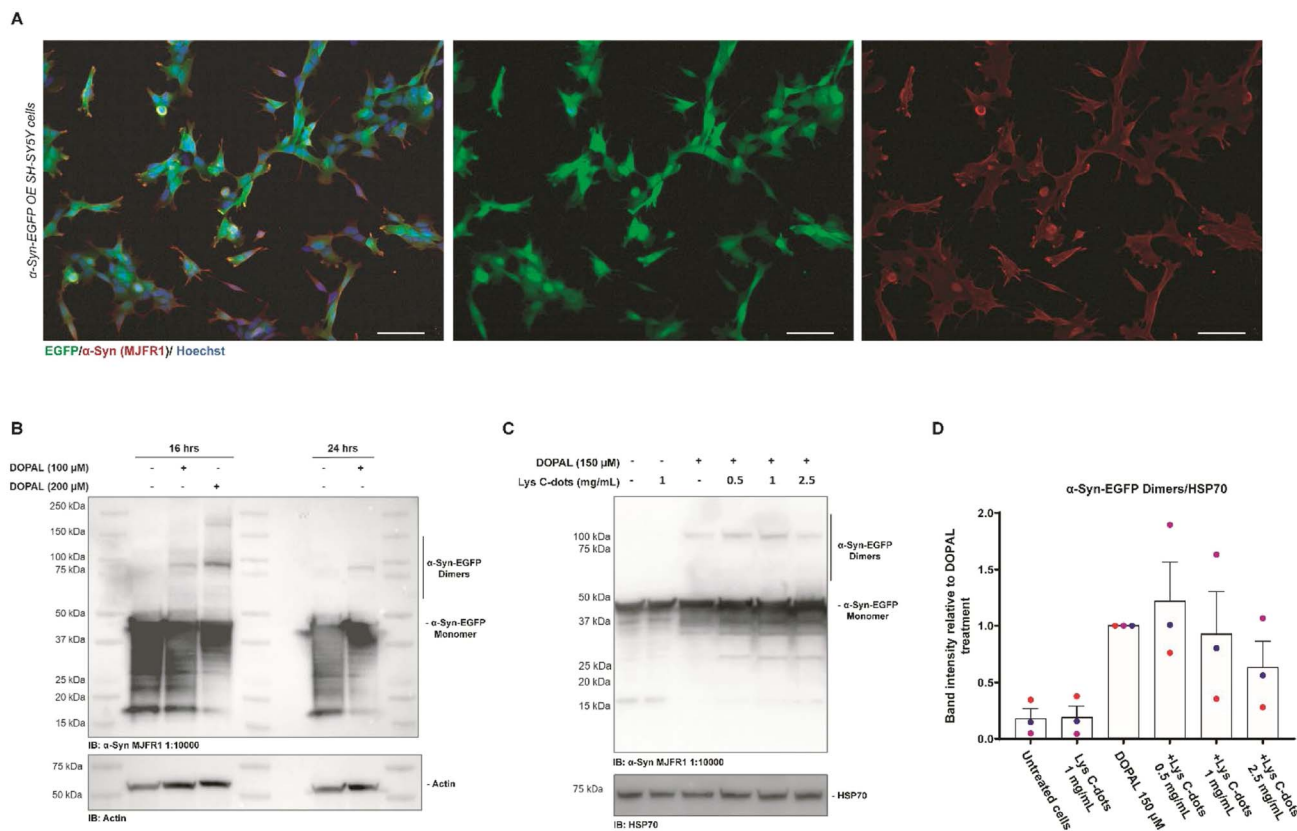
Fig. 8 Validation of the SH-SY5Y stable cell line over-expressing α-Syn-EGFP and recovering of the DOPAL effect by treatment with Lys C-dots. (A) Immunofluorescence of SH-SY5Y stable cells overexpressing α-Syn-EGFP (green) and stained with an anti-α-Syn (MJFR1) antibody (red) to display co-localization. Nuclei are stained with Hoechst (blue), scale bar 50 μM. (B) Western blot of SH-SY5Y cells over-expressing α-Syn-EGFP treated with 100−200 μM DOPAL at different time points (18−24 hours). DOPAL induced dimers revealed by the anti-α-Syn (MJFR1) antibody are detected at 90−100 kDa. (C) Western blot analysis of lysates of SH-SY5Y cells over-expressing α-Syn-EGFP pre-treated with specified concentrations of Lys C-dots for 24 hours, following 150 μM DOPAL treatment for 18 hours. (D) In the quantification, the band intensity of the α-Syn-EGFP dimer was normalized to HSP70. Data are presented as mean ± SEM ($n = 3$).

evaluation in Fig. 8D) demonstrate that the C-dots reduced α-Syn-EGFP dimer generation in a dose-dependent manner. Although the decreased dimerization is not statistically significant, the trend in Lys-C-dot-dependent α-Syn-EGFP dimer reduction was consistent among the three independent experiments.

Taken together, these results demonstrate that Lys-C-dots can reduce cell cytotoxicity and α-Syn aggregation induced by DOPAL, a prominent biogenic aldehyde. In particular, the experimental data underscore the significance of high concentration of amine residues on the surface of the C-dots, which likely play the key role in aldehyde scavenging. DOPAL, like other aldehydes, is highly reactive and can therefore cause cell damage in a variety of ways such as DNA damage, mitochondrial damage, cell membrane destruction, ROS formation and protein damage.[50] Identification of novel, biocompatible, and environmentally benign aldehyde scavenging agents might provide an innovative therapeutic avenue against varied pathological conditions.

In the case of α-Syn, the presence of DOPAL leads to the formation of soluble oligomers which are likely the toxic species of the protein. The formed oligomers are not competent to proceed further in the protein aggregation stages to mature fibrillation. DOPAL affects the physiological roles of the protein and its toxicity, therefore, the effect of DOPAL on α-Syn should be avoided.

Using various spectroscopic and protein analysis methods, we have shown that the presence of Lys C-dots in a solution containing DOPAL and α-Syn can prevent their binding and the effect of DOPAL on the oligomerization of the protein. Our results demonstrate that Lys C-dots also significantly avoid the modification of the α-Syn monomer by DOPAL recovering both the affinity of the protein for SUVs and the formation of helical conformations by α-Syn upon membrane binding. Functionally, C-dots inhibit the formation of the DOPAL α-Syn complex and its membrane interaction and potentially its subsequent effects, such as vesicle permeabilization.[8] The efficient DOPAL scavenging by Lys C-dots was also confirmed by TEM and ThT experiments where C-dot sequestration allows the formation of fibrils despite the presence of the aldehyde.

Our experiments reveal that Lys-C-dots are non-toxic and can penetrate SH-SY5Y cells, reducing cell mortality due to DOPAL toxicity, demonstrated both by XTT assay and GIEMSA staining. In addition, they also partially reduced the formation of

intracellular α-Syn oligomers. Essentially, DOPAL scavenging by Lys-C-dots results in new complexes that are less or not toxic, but more insight will be needed to understand how C-dots are metabolized within the cell both in their normal and DOPAL bound forms.

According to the presented data, it would be interesting to explore the use of Lys C-dots as therapeutic agents in scavenging aldehydes. In fact, as previously reported[51] an amine group is effective to prevent DOPAL induced protein aggregation as a small molecule (*e.g.*, metformin, aminoindan, and hydralazine), but considering our results it functions also as a surface anchored group on C-dots. In the first instance, Lys-C-dots could be effective for the detoxification of MGO, the key α-oxoaldehyde produced under hyperglycemia in the blood of type 2 diabetes patients.[52] In this case the scavenging of MGO, prevention of amino acid modification in proteins, and formation of advanced glycation end products (AGEs)[53] could be achieved directly in the blood after C-dot administration. However, in the case of DOPAL other factors should be considered. Among them, DOPAL is mostly produced in nigrostriatal dopaminergic neurons, and it exerts its toxicity in the central nervous system, and therefore an effective scavenging agent needs to overcome the blood–brain barrier (BBB). C-dots abundant in amine groups on their surfaces are reported to be able to cross the BBB in animal models[54] and as we demonstrated Lys C-dots can penetrate neuron-like cells. These considerations strengthen the potential use of Lys C-dots as effective DOPAL scavengers.

Conclusions

This study demonstrates that C-dots, prepared from lysine as the carbonaceous precursor, effectively inhibit the cytotoxic and protein aggregation activities of DOPAL, a prominent biogenic aldehyde derived from dopamine. We have shown that the ubiquitous amine moieties displayed on the C-dot surface scavenge the aldehyde molecules through interactions with the aldehyde residues. *In vitro* experiments and cell viability analysis reveal that the Lys-C-dots mimicked the scavenging properties of amino groups present in other small molecules used for this purpose. Interestingly, the experiments demonstrate that the Lys-C-dots inhibited α-Syn modification by DOPAL, specifically oligomer formation, and restored vesicle binding and fibril formation. Experiments in SH-SY5Y cells indicated that Lys-C-dots, in addition to being internalized and nontoxic, also reduced DOPAL-mediated cytotoxicity, and also minimized intracellular α-Syn oligomerization. In conclusion, this work illustrates a potential strategy employing amine-displaying C-dots as a vehicle for scavenging of cytotoxic aldehydes and alleviating pathological conditions in PD and other protein misfolding diseases.

Author contributions

Daniel Nir Bloch: investigation, formal analysis, visualization, and writing – original draft. Michele Sandre: conceptualization, investigation, formal analysis, visualization, writing – original draft, and writing – review and editing. Shani Ben-Zichri: investigation. Anna Masato: investigation, formal analysis, writing – review, and editing. Sofiya Kolusheva: formal analysis and visualization. Luigi Bubacco: funding, supervision, and writing – review and editing. Raz Jelinek: funding, supervision, and writing – review and editing.

Conflicts of interest

There are no conflicts to declare.

Acknowledgements

References

1 E. R. Dorsey and B. R. Bloem, *JAMA Neurology*, 2018, **75**, 9–10.

2 A. Masato, M. Sandre, A. Antonini and L. Bubacco, *Curr. Neuropharmacol.*, 2021, **19**, 1618–1639.

3 A. Masato, N. Plotegher, D. Boassa and L. Bubacco, *Mol. Neurodegener.*, 2019, **14**, 35.

4 B. S. Cagle, R. A. Crawford and J. A. Doorn, *Curr. Opin. Toxicol.*, 2019, **13**, 16–21.

5 M. G. Spillantini, M. L. Schmidt, V. M. Y. Lee, J. Q. Trojanowski, R. Jakes and M. Goedert, *Nature*, 1997, **388**, 839–840.

6 N. Plotegher and L. Bubacco, *Ageing Res. Rev.*, 2016, **26**, 62–71.

7 C. Follmer, E. Coelho-Cerqueira, D. Y. Yatabe-Franco, G. D. Araujo, A. S. Pinheiro, G. B. Domont and D. Eliezer, *J. Biol. Chem.*, 2015, **290**, 27660–27679.

8 N. Plotegher, G. Berti, E. Ferrari, I. Tessari, M. Zanetti, L. Lunelli, E. Greggio, M. Bisaglia, M. Veronesi, S. Girotto, M. Dalla Serra, C. Perego, L. Casella and L. Bubacco, *Sci. Rep.*, 2017, **7**, 40699.

9 W. J. Burke, V. B. Kumar, N. Pandey, W. M. Panneton, Q. Gan, M. W. Franko, M. O, Dell, S. W. Li, Y. Pan, H. D. Chung and J. E. Galvin, *Acta Neuropathol.*, 2008, **115**, 193–203.

10 F. Agostini, A. Masato, L. Bubacco and M. Bisaglia, *Int. J. Mol. Sci.*, 2022, **23**, 398.

11 C. Sportelli, D. Urso, P. Jenner and K. R. Chaudhuri, *Front. Neurol.*, 2020, **11**, **https://www.frontiersin.org/articles/10.3389/fneur.2020.00556/full**.

12 F. R. Baptista, S. A. Belhout, S. Giordani and S. J. Quinn, *Chem. Soc. Rev.*, 2015, **44**, 4433–4453.

13 N. Esfandiari, Z. Bagheri, H. Ehtesabi, Z. Fatahi, H. Tavana and H. Latifi, *Heliyon*, 2019, **5**, e02940.

14 D. N. Bloch, S. Ben Zichri, S. Kolusheva and R. Jelinek, *Nanoscale Adv.*, 2020, **2**, 5866–5873.

15 J. Plácido, S. Bustamante-López, K. E. Meissner, D. E. Kelly and S. L. Kelly, *Sci. Total Environ.*, 2019, **656**, 531–539.

16 S. K. Bhunia, A. R. Maity, S. Nandi, D. Stepensky and R. Jelinek, *ChemBioChem*, 2016, **17**, 614–619.

17 S. Dolai, S. K. Bhunia, L. Zeiri, O. Paz-Tal and R. Jelinek, *ACS Omega*, 2017, **2**, 9288–9295.

18 R. Malishev, E. Arad, S. K. Bhunia, S. Shaham-Niv, S. Kolusheva, E. Gazit and R. Jelinek, *Chem. Commun.*, 2018, **54**, 7762–7765.

19 R. Jelinek, Bioimaging Applications of Carbon-Dots, in, *Carbon Quantum Dots, Carbon Nanostructures*, Springer, Cham, 2017, DOI: 10.1007/978-3-319-43911-2_5.

20 S. Zhu, Q. Meng, L. Wang, J. Zhang, Y. Song, H. Jin, K. Zhang, H. Sun, H. Wang and B. Yang, *Angew. Chem., Int. Ed.*, 2013, **52**, 3953–3957.

21 X. Li, S. Zhang, S. A. Kulinich, Y. Liu and H. Zeng, *Sci. Rep.*, 2014, **4**, 4976.

22 Y. Z. Fan, Y. Zhang, N. Li, S. G. Liu, T. Liu, N. B. Li and H. Q. Luo, *Sens. Actuators, B*, 2017, **240**, 949–955.

23 S. Xiangcheng, *TrAC, Trends Anal. Chem.*, 2017, **89**, 163–180.

24 X. Li, M. Rui, J. Song, Z. Shen and H. Zeng, *Adv. Funct. Mater.*, 2015, **25**, 4929–4947.

25 Z. Zhang, T. Zheng, X. Li, J. Xu and H. Zeng, *Part. Part. Syst. Charact.*, 2016, **33**, 457–472.

26 B. Wang, H. Cai, G. I. N. Waterhouse, X. Qu, B. Yang and S. Lu, *Small Sci.*, 2022, **2**, 2200012.

27 I. Tessari, M. Bisaglia, F. Valle, B. Samorì, E. Bergantino, S. Mammi and L. Bubacco, *J. Biol. Chem.*, 2008, **283**, 16808–16817.

28 J. H. Fellman, *Nature*, 1958, **182**, 311–312.

29 D. Cai, J. Qi, Y. Yang, W. Zhang, F. Zhou, X. Jia, W. Guo, X. Huang, F. Gao, H. Chen, T. Li, G. Li, P. Wang, Y. Zhang and H. Lei, *Molecules*, 2019, **24**(22), 4025.

30 M. Jorns and D. Pappas, *Nanomaterials*, 2021, **11**, 1448.

31 B. Unnikrishnan, R.-S. Wu, S.-C. Wei, C.-C. Huang and H.-T. Chang, *ACS Omega*, 2020, **5**, 11248–11261.

32 G. Banfalvi, *Apoptosis*, 2017, **22**, 306–323.

33 E. Bagnoli, T. Diviney and U. FitzGerald, *Eur. J. Neurosci.*, 2021, **53**, 2960–2972.

34 M. Zhu, J. Li and A. L. Fink, *J. Biol. Chem.*, 2003, **278**, 40186–40197.

35 M. Necula, C. N. Chirita and J. Kuret, *J. Biol. Chem.*, 2003, **278**, 46674–46680.

36 L. Tosatto, A. O. Andrighetti, N. Plotegher, V. Antonini, I. Tessari, L. Ricci, L. Bubacco and M. Dalla Serra, *Biochim. Biophys. Acta*, 2012, **1818**, 2876–2883.

37 I. C. Brás, M. Xylaki and T. F. Outeiro, *Prog. Brain Res.*, 2020, **252**, 91–129.

38 P. K. Auluck, G. Caraveo and S. Lindquist, *Annu. Rev. Cell Dev. Biol.*, 2010, **26**, 211–233.

39 K. Nakamura, V. M. Nemani, F. Azarbal, G. Skibinski, J. M. Levy, K. Egami, L. Munishkina, J. Zhang, B. Gardner, J. Wakabayashi, H. Sesaki, Y. Cheng, S. Finkbeiner, R. L. Nussbaum, E. Masliah and R. H. Edwards, *J. Biol. Chem.*, 2011, **286**, 20710–20726.

40 A. Micsonai, F. Wien, L. Kernya, Y. H. Lee, Y. Goto, M. Réfrégiers and J. Kardos, *Proc. Natl. Acad. Sci. U. S. A.*, 2015, **112**, E3095–E3103.

41 S. Kitagawa, M. Matsubayashi, K. Kotani, K. Usui and F. Kametani, *J. Membr. Biol.*, 1991, **119**, 221–227.

42 M. Suzuki and T. Miura, *Biochim. Biophys. Acta*, 2015, **1848**, 753–759.

43 C. Xue, T. Y. Lin, D. Chang and Z. Guo, *R. Soc. Open Sci.*, 2017, **4**, 160696.

44 K. Gade Malmos, L. M. Blancas-Mejia, B. Weber, J. Buchner, M. Ramirez-Alvarado, H. Naiki and D. Otzen, *Amyloid*, 2017, **24**, 1–16.

45 L. Giehm, N. Lorenzen and D. E. Otzen, *Methods*, 2011, **53**, 295–305.

46 J. H. Torpey, R. M. Meade, R. Mistry, J. M. Mason and J. Madine, *Front. Neurol.*, 2020, **14**, https://www.frontiersin.org/articles/10.3389/fnmol.2021.659926/full.

47 Y. Jinsmaa, P. Sullivan, Y. Sharabi and D. S. Goldstein, *Auton. Neurosci.*, 2016, **194**, 46–51.

48 Y. Jinsmaa, P. Sullivan, D. Gross, A. Cooney, Y. Sharabi and D. S. Goldstein, *Neurosci. Lett.*, 2014, **569**, 27–32.

49 J. R. Mazzulli, M. Armakola, M. Dumoulin, I. Parastatidis and H. Ischiropoulos, *J. Biol. Chem.*, 2007, **282**, 31621–31630.

50 A. Ahmed Laskar and H. Younus, *Drug Metab. Rev.*, 2019, **51**, 42–64.

51 V. B. Kumar, F.-F. Hsu, V. M. Lakshmi, K. N. Gillespie and W. J. Burke, *Eur. J. Pharmacol.*, 2019, **845**, 65–73.

52 C. G. Schalkwijk and C. D. A. Stehouwer, *Physiol. Rev.*, 2020, **100**, 407–461.

53 A. Reyaz, S. Alam, K. Chandra, S. Kohli and S. Agarwal, *J. Diabetes Metab. Disord.*, 2020, **19**, 515–521.

54 W. Zhang, G. Sigdel, K. J. Mintz, E. S. Seven, Y. Zhou, C. Wang and R. M. Leblanc, *Int. J. Nanomed.*, 2021, **16**, 5003–5016.